

SMART Hawk: A Shape-Morphing Artificial Red-Tailed Hawk [†]

Peter L. Bishay ^{*}, Leo Haroutoonian, Victoria Bures, Caleb Wilmarth, Chaya Rubinstein, Arman Geghamyan, Gustavo Vela, Nico Alexander, Evelyn Herrera, Christian Guerrero, Cassidy Lai, Angelina Argott, Rogelio Banales, Johnathon Moore, Alicia Schwartz, Levon Ananyan, Adrian Gutierrez Corral and John Cannon

Department of Mechanical Engineering, California State University, Northridge, CA 91330, USA;

^{*} Correspondence: peter.bishay@csun.edu

[†] Presented at the first International Online Conference on Aerospace Engineering (IOCAE), 16–17 April 2026.

Abstract

Birds actively modulate their wing and tail morphologies to achieve high aerodynamic efficiency and maneuverability, enabling long-duration gliding while retaining the ability to execute rapid maneuvers. Innovations in aircraft design and control are increasingly inspired by these avian flight characteristics through control surfaces that imitate the natural wing and tail movements of birds. This paper presents a non-flapping, unmanned aerial vehicle (UAV), called “SMART Hawk” (Shape-Morphing Artificial Red-Tailed Hawk), inspired by the flight and physical characteristics of *Buteo jamaicensis*, known as the Red-Tailed Hawk (RTH), which exhibits excellent soaring abilities and agility characteristic of birds of prey. To determine the design parameters required for flight, a mathematical model was developed in MachUpX, then validated and refined using Reynolds-averaged computational fluid dynamics (CFD) models in ANSYS Fluent. SMART Hawk incorporates biomimetic wing and tail morphing, including coordinated forward sweep of the mid-wing and aft sweep of the outer wing, as well as active tail pitch, roll, and feather tucking and expansion. The drone was manufactured from a combination of composite, wood, and 3D-printed components. Multiple flight tests were conducted with proof-of-concept prototypes to demonstrate the design’s effectiveness.

Keywords: morphing wings; bioinspiration; non-flapping drones

1. Introduction

Birds have served as a source of inspiration for aircraft design for over a century [1]. They are capable of seamlessly morphing their wings and manipulating their tails to achieve precise and controlled flight. Hawks, in particular, can sustain efficient gliding flight while rapidly transitioning to aggressive maneuvers such as dives, making them among the most effective flyers in nature. Red-tailed hawks (RTHs) specifically possess long, broad wings that enable extended soaring followed by tight, agile maneuvers to capture prey [2]. Recent studies of RTH flight have examined their adaptability in turbulent environments, showing that they pitch their wings and tails to mitigate the effects of gusts [3]. Birds achieve such seamless flight through specialized biological structures and mechanisms. Understanding the mechanisms by which they tuck their wings has been critical to the development of morphing drones, as these natural strategies directly inform engineered solutions [4].

Academic Editor(s): Name

Published: date

Copyright: © 2026 by the authors.
Submitted for possible open access
publication under the terms and
conditions of the [Creative Commons
Attribution \(CC BY\) license](#).

It is difficult to fully capture the agility, aerodynamic efficiency, dimensions, and material properties of a bird in a manufactured drone. A wide section of biomimetic research focused on developing a single avian-inspired morphing component for a traditional airplane. Ajanic et al. [5] developed a bionic wing modeled after a jackdaw able to flap, pitch, and fold. Murayama et al. [6] presented a tail capable of tail pitch, tilt, and rudder motion. Zhang et al. [7] analyzed a shape-morphing avian-inspired wing. Various studies sought to develop a morphing unmanned aerial vehicle (UAV) inspired by different avian species. Ajanic et al. [8] demonstrated the effects of asymmetric wing tucking, compared to outer wing pitching, as a means of reducing the turning radius of LisEagle, a feathered morphing drone inspired by eagle flight. Chang et al. [9] incorporated real pigeon feathers into the design of PigeonBot II and successfully demonstrated flight without a vertical stabilizer or rudder. Phan and Floreano [10] incorporated an entirely artificial, feathered-wing design comprising three segmented wing components in their Raptor drone, enabling wing and tail shape morphing, tail elevator deflection, roll, and lateral deflection. Other artificially feathered bioinspired drones, including MataGull [11] and CGull [12], both inspired by seagulls, also featured tail and wing morphing.

One of the greatest challenges in designing drones with morphing and feathered wings and tails is the increased potential of fluttering when joints are introduced in the wing structure. Reinforcing the morphing structures can easily introduce weight penalties. To address these challenges, this paper presents a UAV inspired by the flight characteristics of the RTH. The drone, named SMART Hawk (Shape-Morphing Artificial Red-Tailed Hawk), is designed to incorporate five degrees of freedom (DOFs): two in the wings to enable asymmetric wing tucking, and three in the tail to allow pitch, roll, and feather expansion. A feathered wing and tail configuration is implemented to more closely replicate the morphology of a real bird. The wing and tail systems, including the morphing mechanisms and the feathers, were designed to be lightweight yet possess high specific stiffness to avoid flutter under aerodynamic loads. The rest of the paper is organized as follows: Section 2 details the preliminary computational model developed in various software packages. Section 3 describes all components and subsystems of SMART Hawk. Section 4 presents the manufacturing and testing steps that were completed. A summary and conclusion are given in Section 5.

2. Computational Modeling

The aerodynamic analysis and validation workflow for SMART Hawk was started using simple calculations in a developed MATLAB code (MATLAB version 2025b), followed by a representative model in MachUpX, and was validated with high-fidelity simulations in ANSYS Fluent (version 2025 R2). The mathematical model provides preliminary analysis for the sizing of the drone's lifting surfaces and evaluates the proposed wing-tucking concept intended to improve flight efficiency. A 3D scan of an RTH cadaver served as a baseline for the developed mathematical model. A representative wing cross-section (airfoil) was extracted from the 3D scan for analysis and use in the model. A maximum reported RTH mass of 1.5 kg was used, along with a conservative low-end cruise flight speed of 10 m/s [13]. An aspect ratio (AR) of 5.6 was also assumed [3]. MachUpX (MUX) uses Prandtl lifting-line theory to output approximate values of the generated aerodynamic forces and moments from the drone's specified planform. The MUX model is transferred to ANSYS Fluent to verify the outcomes and investigate the effects of the design parameters on the predicted aerodynamic performance of the entire feathered drone.

2.1. Airfoil Analysis and Preliminary Planform Modeling

The RTH airfoil cross-section, unique to this study, was smoothed in MATLAB from the rough profile extracted from the RTH cadaver 3D scan. The smoothed profile, shown

in Figure 1a, was analyzed in Xfoil to create 2D aerodynamic polars under specific flow conditions. The fluid environment model within Xfoil uses a Reynolds number (Re), calculated based on the following parameters: Density (ρ): 1.246 kg/m³, dynamic viscosity (μ): 1.85×10^{-5} Pa·s, velocity (v): 10 m/s, and an initial chord length of 30 cm, leading to Re : 202,054. The Rhodes St. Genese 32 (RSG32) airfoil (Figure 1b) was used for the inner wing section given its flat-bottom geometry, simplifying manufacturing while maintaining adequate aerodynamic performance with respect to lift and stall angle. Figure 1c,d present lift coefficient and aerodynamic efficiency of the RTH airfoil versus angle of attack (AOA, α) for the considered Re , assuming an infinite-span section. The coefficient fits of the airfoil were used in MUX to iteratively size the SMART Hawk lifting platform.

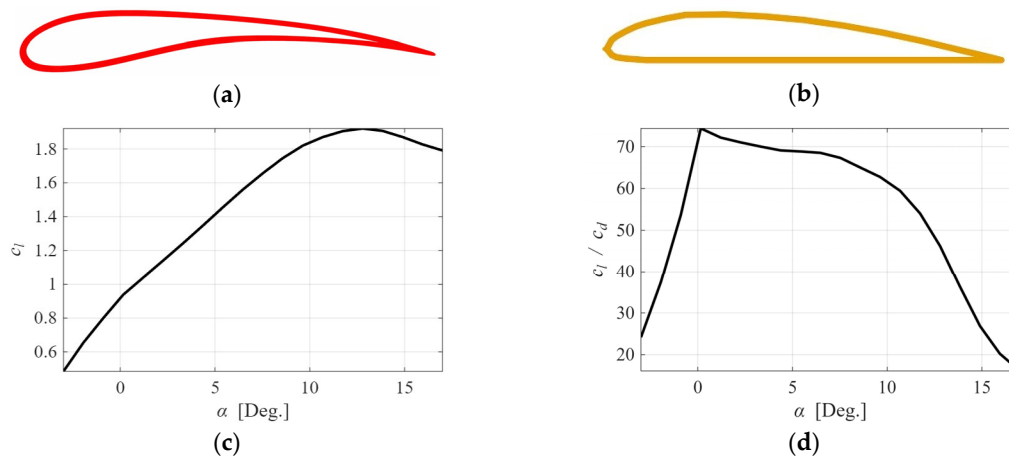


Figure 1. (a) RTH airfoil outline; (b) RSG32 airfoil outline; (c) RTH lift coefficient; (d) RTH flight efficiency.

From the $c_l - \alpha$ curve obtained in Xfoil, the lift curve slope (a_0) and the zero-lift AOA ($\alpha_{L=0}$) were obtained as $a_0 = 0.1$ and $\alpha_{L=0} = -4^\circ$. An AOA, α , of 4.4° was selected as the design cruise AOA to maximize efficiency. The Oswald efficiency factor is assumed to be 1 for elliptical wings, $e = 1$. The lift coefficient for the finite wing, C_L , can be calculated as

$$C_L = \frac{a_0}{1 + \frac{a_0}{\pi e AR}} (\alpha - \alpha_{L=0}) \quad (1)$$

The wing planform area S can be calculated from the lift equation, assuming a level flight:

$$L = \frac{1}{2} \rho v^2 S C_L \quad (2)$$

The wingspan can then be obtained using the AR definition, $AR = b^2/S$. Finally, the root chord length can be obtained using the elliptical wing area formula, $S = \pi b c_r / 4$. Here, the preliminary wingspan and chord length were found to be $b = 1.21$ m and $c_r = 0.297$ m.

Using the analytically estimated span and chord, a planform was created and iteratively refined in MUX. The wings were swept forward 5° and a twist of 5° was implemented to the outer wings to delay stall onset. The resulting configuration is shown in Figure 2a, which includes the tail model to quantify loads under control-surface deflection. Figure 2b,c show the lift coefficient and the flight efficiency of the airframe as a function of AOA. It was found that the AOA that maximizes aerodynamic efficiency is $2\text{--}3^\circ$.

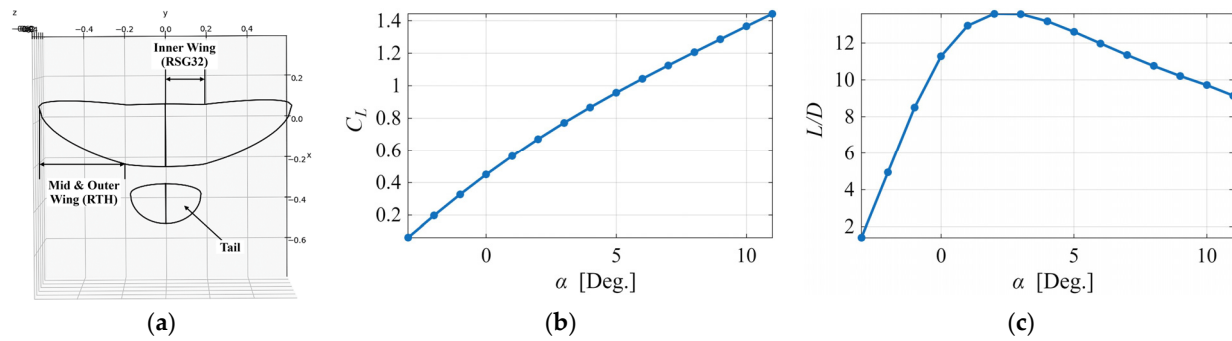


Figure 2. (a) MUX airframe, (b) lift coefficient, and (c) flight efficiency of the MUX model.

2.2. Design Concept Evaluation

Following preliminary modeling in MUX, the configuration was transferred to ANSYS Fluent. This enabled validation of the MUX predictions and evaluation of the higher-fidelity configuration, including feathered wings, wing-tucking, and tail morphing, to assess their aerodynamic interaction. Turbulence closure was provided by the $k-\omega$ family using the SST framework for high-quality near-wall resolution and reduced free-stream sensitivity [14].

The half-wing model met the target lift of 7.35 N and produced approximately 0.1 N of overall drag. A model of the full drone, including the wings, tail, and fuselage, was then created. A nose cone was added to the fuselage to reduce drag, changing the fuselage cross-section from a blunt nose to a streamlined, airfoil-like 2D cross-section. This increased the total lift by 1.8 N. The wing planform was transitioned from the idealized planform represented in MUX to the final design model with feathers proposed in this study. Mesh refinement yielded an orthogonality minimum of 0.150 and a skewness maximum of 0.850 for the model and its environment. The full configuration (Figure 3a) is simulated using the framework above, yielding 14.7 N of lift and 1.2 N of total drag at 10 m/s and an AOA of 5° . A representative pressure contour is shown in Figure 3b, whereas top and bottom views are shown in Figure 3c and d, respectively. The simulations showed the effects of the orientation angles of all feathers, and the shape of the leading edge covers on the generated lift and drag. The simulations helped make design adjustments that resulted in feather orientations more closely aligned with the RTH profile, thereby enhancing aerodynamic performance.

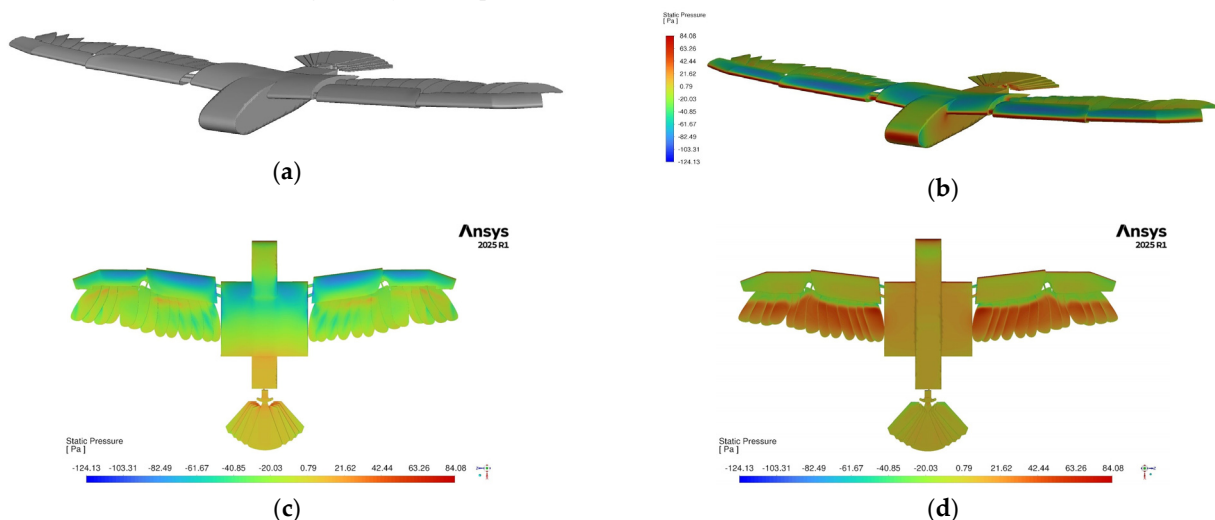


Figure 3. ANSYS model: CAD model (a), and isometric view (b), top view (c), and bottom view (d), of the pressure contours.

3. Model Description

3.1. Overall Design

The complete SMART Hawk model is shown in Figure 4. It is divided into three primary subassemblies (fuselage, wings, and tail) and incorporates five degrees of freedom: asymmetric wing tucking, tail feather expansion, rolling, and pitching. Mounted on top of the fuselage, the wings can induce roll through an asymmetric change in both the wing planform area and sweep. Mimicking the RTH, the wing mechanism features a replicated avian bone structure and feathers. The fuselage possesses an airfoil cutout where the wings sit to guide airflow onto the top of the wings. The fuselage houses all avionic components in addition to the wings' tucking servomotors. The tail, actuated using servomotors located inside the fuselage through pullrods and guitar wires, can induce roll and pitching moments. The drone follows the dimensions set by the MUX model.

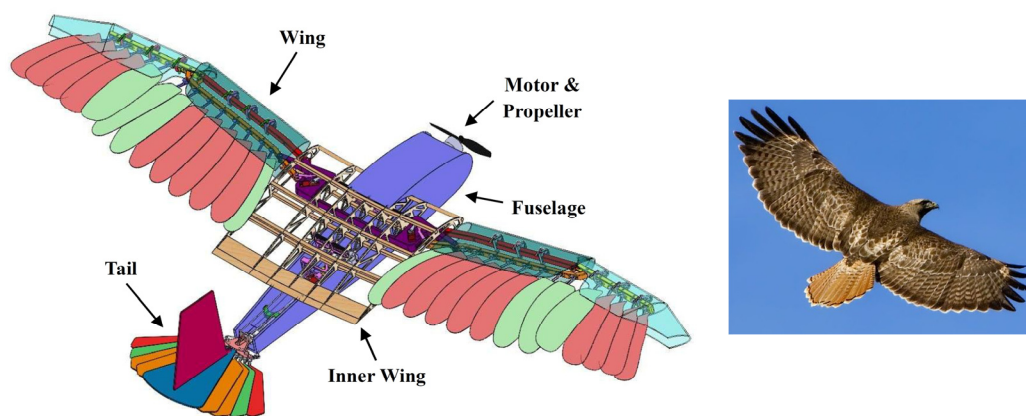


Figure 4. Full CAD model of SMART Hawk [the bird figure is photographed by Dan Hutcheson].

3.2. Wing Design

The wing assembly consists of the inner wing structure, wing covers, actuation mechanism, and feathers, as shown in Figure 5a. A 5° dihedral is incorporated into the wings to provide higher roll stability, and a 5° twist is applied to the outer 15% of the wings to increase the stall angle. The wings are composed of a tucking mechanism, making up 76% of the total wingspan, and a fixed inner wing, which is attached to the top of the fuselage. The mechanism, which integrates carbon fiber feathers and covers, enables asymmetric wing tucking with an area reduction of 22.5%.

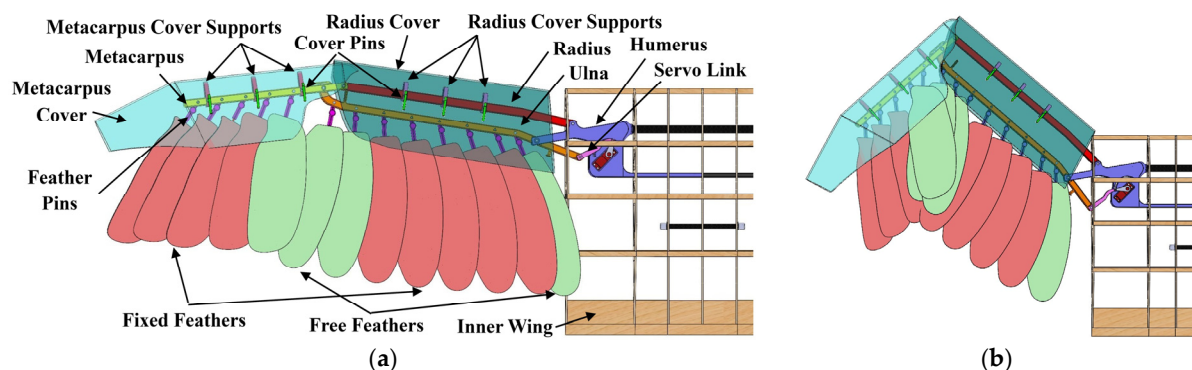


Figure 5. (a) SMART Hawk's wing design in extended wing configuration and (b) tucked configuration.

Inspired by avian skeletal anatomy [15], the mechanism incorporates elements analogous to the humerus, radius, ulna, and metacarpus, along with a link arm. Components are 3D-printed in PLA-CF with a 15–30% gyroid infill and two to four perimeter walls to balance the weight-to-strength ratio. The RTH airfoil profile was applied to the morphing wing section, with the covers replicating the RTH geometry and the mean camber profile incorporated into the curved feather elements. Carbon fiber covers form the leading 30% of the chord and are attached to the metacarpus and radius using PLA pins, while stiff fabric bonded along the underside bridges the gap to the feathers to mitigate vortex-induced flutter that was reflected in the computational model results. Additional PLA airfoil supports connect the covers to the metacarpus and radius to provide additional structure. The feathers are attached via PLA pins to the ulna and metacarpus, with thirteen feathers per wing, eight on the ulna and five on the metacarpus, for a total of 26 feathers. Three distinct feather geometries were used, traced from RTH feathers [16,17] to replicate the shapes of primary and secondary feathers. Of the thirteen feathers on each wing, nine are rigidly fixed, while four are free to rotate in yaw to enable smooth tucking among the feathers that span the gap across the metacarpus and ulna while reducing the risk of flutter. Orthodontic rubber bands link the free-rotating feathers, acting as elastic springs to return them to position when the wing is actuated back into an extended position. Figure 5b shows the fully tucked wing configuration.

The inner wing assembly, shown in Figure 6, is built from balsa and basswood ribs, stringers, and a trailing-edge plank, along with an 8 mm carbon fiber rod serving as the main spar, a PLA-CF humerus, and a secondary, smaller 6 mm carbon fiber spar. The fixed humerus houses an MKS HV6150H servomotor, which actuates the wing tucking and expansion motion through a link connected to the ulna. The airfoil profile of the inner wing is the RSG32. A 5° dihedral is applied along the inner wingspan, excluding the central three-rib section that rests on the fuselage. The primary 8 mm carbon fiber spar connects to the wing–fuselage bracket, which anchors the wing to the fuselage, while a shorter 6 mm carbon fiber rod near the inner wing’s trailing edge provides additional structural support and serves as a secondary attachment point to the fuselage.

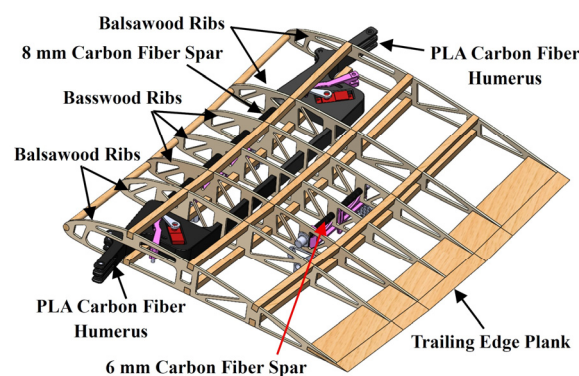


Figure 6. SMART Hawk’s inner wing.

3.3. Fuselage Design

The fuselage functions as the body of the drone that accommodates the avionics, tail assembly, and wing assembly, as shown in Figure 7. The fuselage consists of a body with an RSG32 airfoil cutout on its top to integrate the inner wing assembly and facilitate a smooth aerodynamic transition to the upper surface of the inner wing. A tapered rear section is incorporated at the end of the fuselage to reduce weight, with the upper surface sloping downwards to promote smoother airflow from the inner wing’s trailing edge to the tail. The fuselage has a long, flat underside near the front to house larger, more

sensitive avionic components and facilitate center of gravity (CG) adjustments. The motor mount, wing-to-fuselage mounts, and tail roll brackets are housed within the fuselage to mount the main components of the drone. The motor mount is located inside the front of the fuselage and maintains one degree of right thrust and two degrees of downthrust for the motor. The wing-to-fuselage mounts are secured to the inner wing using carbon fiber spars in the wing assembly and wooden dowels that pass through the fuselage body. Fuselage clamp brackets provide additional reinforcement for the dowel connections, and tail roll brackets support and stabilize the tail rolling rod. The pitch and tuck servo bracket attaches to the tail rolling rod and houses the servomotors that control the pitch and feather expansion/tucking of the tail.

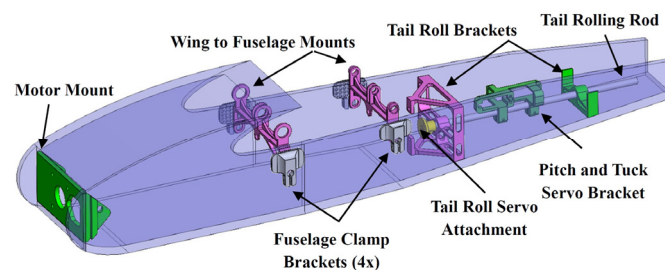


Figure 7. SMART Hawk's fuselage.

3.4. Tail Design

The tail assembly is composed of a tail feather bracket, feather pins (or connectors), a pitching hinge, feathers, and a vertical stabilizer, as shown in Figure 8. The tail is capable of three degrees of freedom: pitching, rolling, and feather expansion. The tail bracket supports nine tail feathers: two outer, two middle, four inner, and one centrally fixed feather, with size decreasing from the central feather (largest) outward to the outer feathers (smallest), as shown in Figure 8b. Eight of the feathers are free to rotate, while the central feather is rigidly attached to the tail bracket. The tail spreads between 80° and 120°, resulting in a 45% area change between the tucked and extended positions. Each of the feathers is made of 2 mm thick balsa wood and 2 mm diameter carbon fiber rods with composite wet lay-up used for additional support. The tail bracket, feather connectors, and pitching hinge are made of PLA with a gyroid infill of 15%. A guitar wire, connected to the outer tail feather pins, is fed through polytetrafluoroethylene (PTFE) tubing on either side of the pitching hinge. After passing through the hinge, the wire ends meet at the center line of the fuselage and are mechanically crimped together to create a single actuation point. This arrangement ensures that when the DS-843MG servo applies tension, the load is distributed symmetrically to both outer feathers, allowing them to spread evenly about the tail centerline. Orthodontic rubber bands interconnect the feathers and function passively to return them to their neutral tucked position once the mechanism is disengaged. The tucked tail configuration is shown in Figure 8c.

Tail pitching is achieved using a servo-driven four-bar linkage. In this system, the tail feather bracket functions as the rocker and is connected to a 1.5 mm steel control rod that acts as the coupler. The rod extends forward to an MKS HV6150H servo arm, which serves as the crank and is mounted inside the fuselage, as shown in Figure 8a. To increase actuation authority, the tail feather bracket features a raised pivot point driven by the steel control rod. Tail roll is controlled by a DS-843MG servo located within the fuselage and connected to a 6 mm carbon fiber torque rod bonded to the pitching hinge. This configuration allows the servo's rotational motion to be transmitted directly to the tail feather bracket, producing controlled rolling movement.

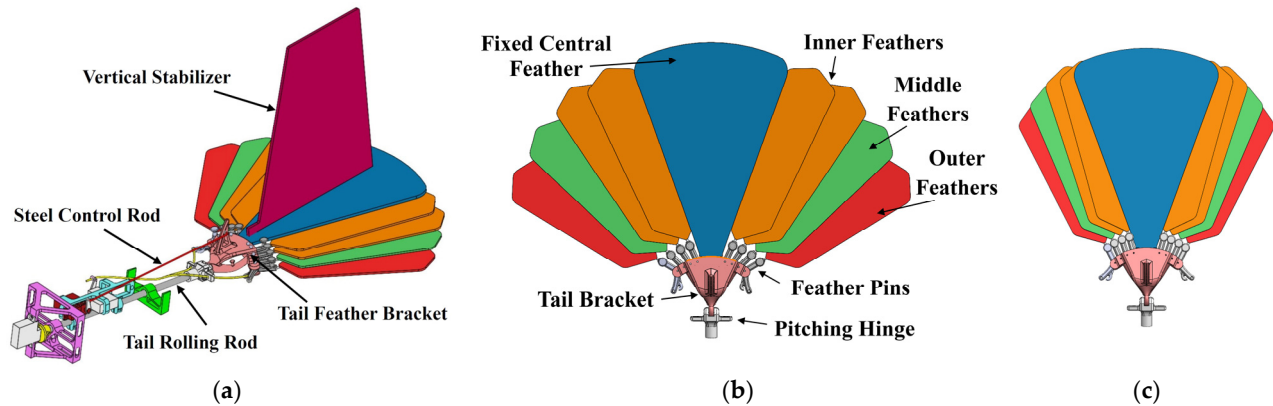


Figure 8. (a) SMART Hawk's tail design; (b) extended tail configuration; (c) tucked tail configuration.

3.5. Avionics and Propulsion System

The SMART Hawk's avionics system, shown in Figure 9a, is composed of the MATEKSYS F405 Wing V2 flight controller, the Corona DS-843MG and MKS HV6150 servomotors, the MATEKSYS GPS and Compass, the FRSKY X8R receiver, and the ESP32 microcontroller. The flight controller acts as the central processing unit, integrating its built-in gyroscope, accelerometer, barometer, and peripherals to collect flight data. For ground monitoring and mission management, the system runs ArduPilot firmware and uses Mission Planner (Version 1.3.83) as the ground control software. Telemetry communication between the aircraft and ground station is established via Wi-Fi, enabled by the ESP32 microcontroller. To fly the model manually and with fly-by-wire, the Taranis QX7 transmitter communicates with the receiver using the control configuration shown in Figure 9b. The transmitter controls are adjusted for the unique biomimetic morphing control surfaces. Aileron control is replaced by wing tucking, and rudder control is replaced by tail tilting.

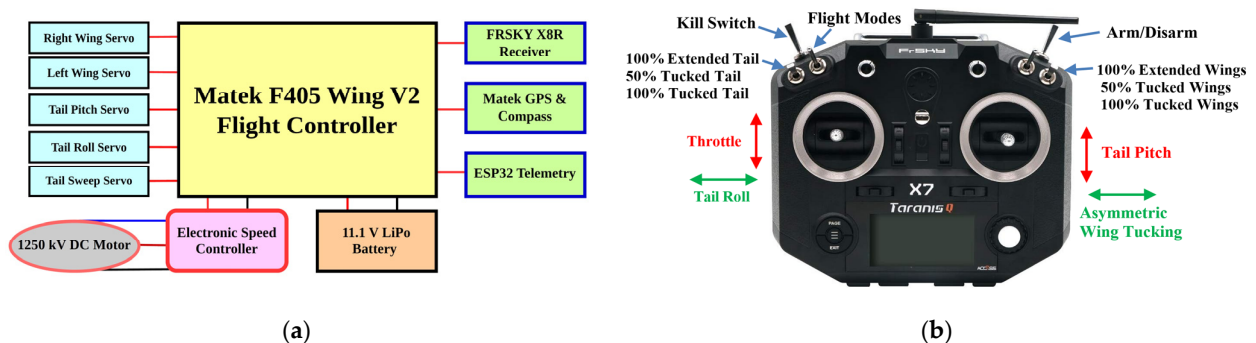


Figure 9. (a) SMART Hawk's avionics diagram; (b) Transmitter controls' configuration.

Because SMART Hawk uses a non-flapping design, propulsion is provided by an E-flite Power 25 brushless outrunner motor (1250 kV), rated for aircraft weighing 1.4–2.5 kg. The motor drives an APC 11 × 5.5 propeller and is controlled by a FlyDragon 60A electronic speed controller (ESC) with an integrated 5A battery eliminator circuit (BEC). Power is supplied by a 3S (11.1 V), 3.0 Ah high-performance lithium–polymer battery. A 2-degree downthrust and a 1-degree right-thrust are engineered into the motor mount to counteract the pitch-up moment from the lowered CG and the adverse yaw moment caused by the vertical stabilizer.

4. Manufacturing and Testing

The process of manufacturing the wing feathers began with a high-density foam mold designed in SOLIDWORKS, then exported to Autodesk Fusion for toolpath generation, and machined on a CNC router, after which the mold was sanded and coated with Duratec to achieve a smooth surface finish. Once the primary mold was fully prepared, a wet layup process was followed to apply seven plies of fiberglass and high-temperature epoxy to produce a secondary mold capable of withstanding elevated temperatures during subsequent prepreg fabrication. Prepreg carbon fiber was selected over traditional wet layup carbon fiber due to its controlled resin content and optimal fiber-to-resin ratio. The feather geometry was cut from carbon fiber prepreg using 3D-printed stencils laid onto the fiberglass mold to form the cambered feathers, as shown in Figure 10a,b. Aluminum rods acted as the shaft of each feather and were selected for their favorable stiffness-to-weight ratio and ease of bending. Each feather consisted of two plies of carbon fiber with a reinforcement strip laid on top of the sandwiched rod.

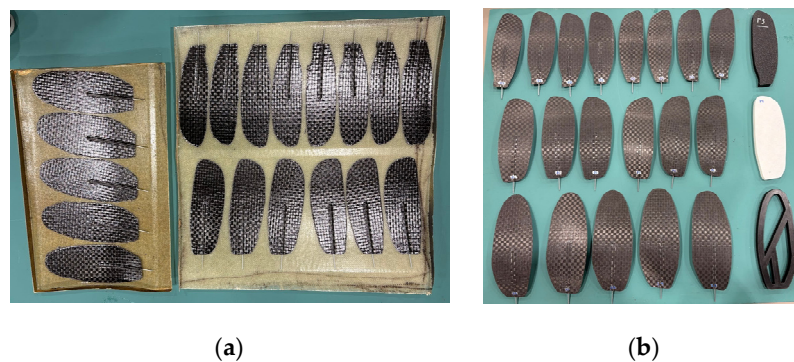


Figure 10. (a) Fiberglass mold with feathers; (b) S9-, P3-, and P1-cured prepreg CF wing feathers with their 3D-printed stencils.

The wing cover molds were manufactured following a similar process. The wing cover molds were 3D-printed due to time efficiency and their complex geometry, then sanded and coated with Duratec (Figure 11a). The same wet layup process was used for manufacturing, with five plies of fiberglass to create a secondary mold (Figure 11b). The wing covers were made with three plies of plain weave carbon fiber prepreg placed inside the fiberglass mold to achieve the desired shape (Figure 11c). Aircraft fabric was used to bridge gaps and create a continuous aerodynamic surface between the wing covers and inner wing, with additional fabric applied along the underside of the trailing edge and reinforced by chordwise carbon fiber rods to provide structural support and reduce vortex formation identified in prior modeling.

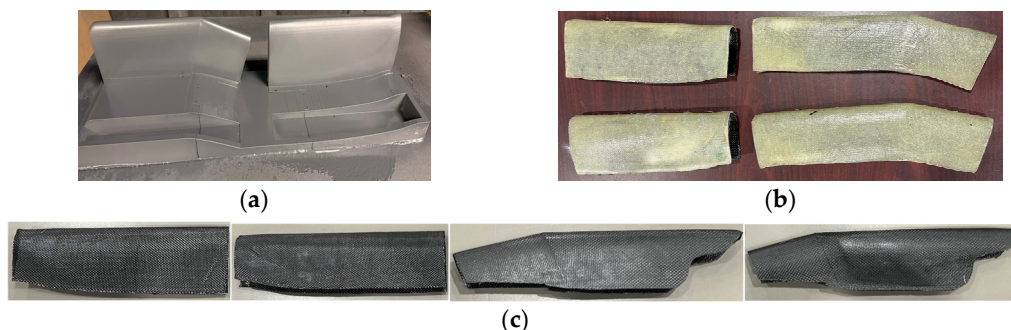


Figure 11. (a) Wing cover molds; (b) fiberglass wing cover molds; (c) CF wing covers.

The inner wing structure was built from balsa and basswood ribs and stringers, assembled around the humerus, which was positioned first. The stringer components were soaked in warm water and dried at a preset angle to achieve a 5° dihedral. The framework was then covered with UltraCote to form the airfoil shape.

The fuselage was constructed from foamboard due to its low weight and rapid manufacturability, allowing the fuselage airfoil profile to be cut and shaped efficiently using CAD-generated templates. The airfoil cross-section for the wing insertion was cut using precision blades to achieve the desired airfoil contour. To reinforce the fuselage structure and provide adequate load transfer between the fuselage and wing assembly, wooden dowel attachments were inserted perpendicular to the internal walls. 3D-printed brackets were glued to the fuselage walls, acting as C-clamps, allowing for quick wing removal and accurate mounting.

The tail feathers were laser cut from 2 mm balsa wood to ensure dimensional accuracy and repeatability, with balsa selected for its low density and adequate stiffness for aerodynamic loading. A single-ply carbon fiber patch was bonded to the balsa using epoxy resin through a wet layup process to attach a 2 mm carbon fiber rod to each feather, as shown in Figure 12a. Epoxy resin was selected for this interface due to its superior bonding strength compared to cyanoacrylate adhesives and for the added stiffness that resulted from the absorption of resin in the balsa feather. The fixed horizontal feather had two carbon fiber rods bonded at each end to provide additional structural support to the balsa wood. A precision slit was cut into the horizontal fixed feather to allow a vertical stabilizer to sit on two PLA brackets. This vertical stabilizer is added for stability during preliminary flight tests. To further increase stiffness, two carbon fiber rods were bonded to the vertical stabilizer (one from each side) along with the two PLA support brackets, as shown in Figure 12b.

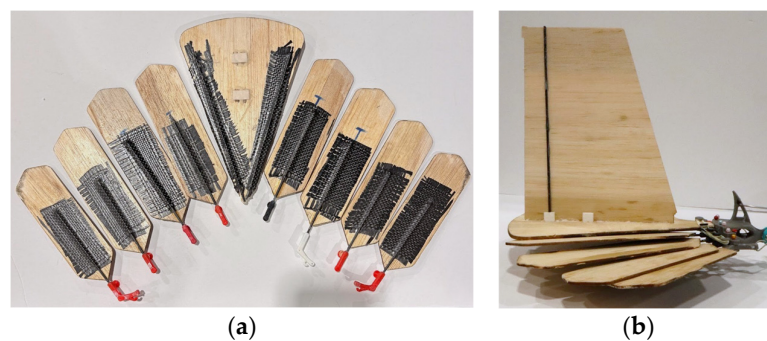


Figure 12. (a) CF wet layup on tail feathers; (b) side view of tail assembly.

Actuation tests on wing and tail morphing were conducted, as seen in Figure 13. All servomotors successfully actuated the wing and tail mechanisms from expanded to fully tucked positions. The tests were also performed when the models were placed in an air-flow generated by a wind generator with a wing speed close to the maximum drone's air speed. This qualitative low-speed airflow exposure test was conducted to observe feather and wing vibration behavior under forced airflow conditions. Actuations were consistent in all tests conducted which exceeded 50 times for each morphing action. The preliminary bench-top airflow excitation test did not show any visually observable large-amplitude oscillations in the feathers, the outer wing structure, or the tail structure, throughout the one-minute duration of the test. A top view of SMART Hawk prototype assembly can be seen in Figure 14. The weight of the initial SMART Hawk prototype is 1.67 kg. Weights of individual components are as follows: fuselage: 65 g, tail structure: 130 g, single wing with servos: 870 g, single wing primary and secondary feathers: 6 and 8 g, respectively, and a

single tail feather: 4.2–7.2 g. The CG is positioned at 23% of the inner wing chord measured from the leading edge, a location identified through multiple morphing-tail flight tests as optimal for providing sufficient tail pitch authority.

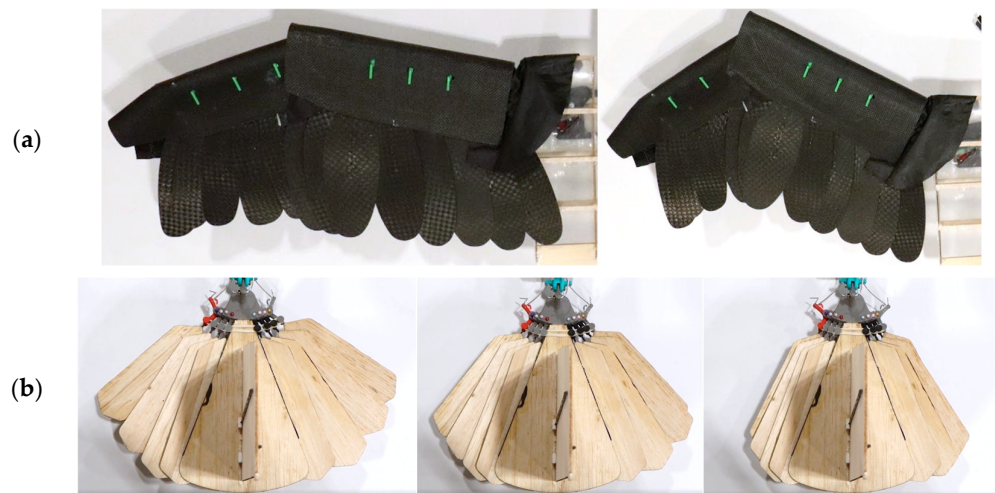


Figure 13. (a) Wing tucking actuation; (b) tail feather spreading actuation.

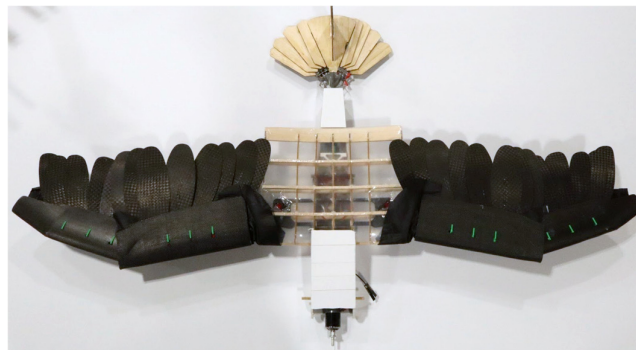


Figure 14. SMART Hawk assembly top view.

Given SMART Hawk's unique control surfaces, an iterative approach was used to characterize the control signals and achieve flight stability. As shown in Figure 15a, a basic aircraft model with traditional tail and wings, having the same tail and wing surface area, was mounted on the SMART Hawk fuselage. After achieving proficient control with this conventional model, the SMART Hawk tail replaced the traditional tail (Figure 15b), followed by the SMART Hawk wings with a traditional tail (Figure 15c), culminating in the final iteration with both morphing wings and tail (Figure 15d).

The intended flight plan consists of a one-minute flight sequence in which the SMART Hawk takes off through hand launch, ascends, and achieves stable flight before executing asymmetric left wing tucking for a full 360-degree turn, followed by asymmetric right wing tucking for another 360-degree turn. The drone then performs symmetric wing tucking to initiate a dive, levels out, and completes a controlled landing. All flight tests were conducted at the Apollo XI model aircraft field, Lake Balboa, CA. Weather conditions during all flight tests were as follows: temperature high ~76 °F, low ~56 °F; wind speed 4–10 mph, with occasional mild gusts up to 12 mph; precipitation 0.0 inch; and humidity 45–50%.

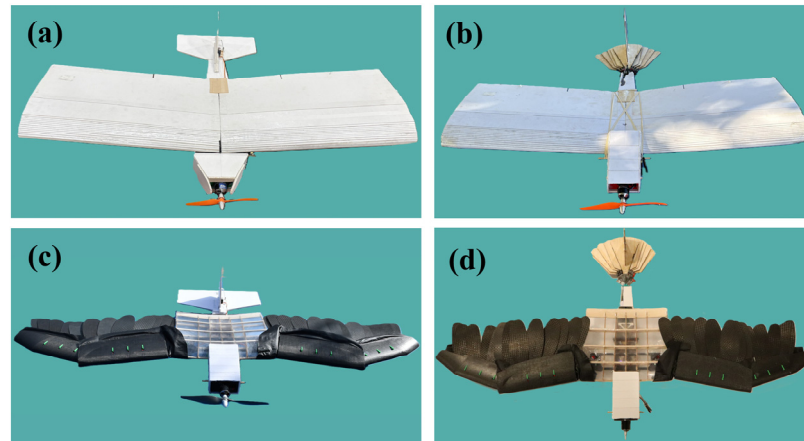


Figure 15. (a) Traditional wing & tail, (b) traditional wing & SMART Hawk tail, (c) SMART Hawk wings & traditional tail, and (d) SMART Hawk.

The traditional drone of the same approximate size and avionic system was initially tested (Figure 16a). A more complex flight plan was executed with this drone with the help of a licensed and experienced RC plane pilot. The morphing tail was then added to the drone, replacing the traditional tail. Flight testing of this drone (Figure 16b) demonstrated the ability to steer the drone using only tail morphing, creating banking angles and turns without ailerons, and landing safely during multiple flight tests, each exceeding two minutes of flight time. Each of the initial two flight tests of SMART Hawk, shown in Figure 16c, achieved a total flight time of 10 s. During the first flight test, the pilot reported difficulty maintaining roll stability due to minor asymmetry in the wings that caused the aircraft to tilt during takeoff. In the second flight test, SMART Hawk successfully flew along a straight path. However, the pilot was unable to carry out a banked turn which led to the aircraft rapidly losing altitude. This result suggests that additional pilot training and familiarization is needed to control SMART Hawk's unconventional control surfaces. Video S1 in the Supplementary Materials shows some of the performed flights tests.

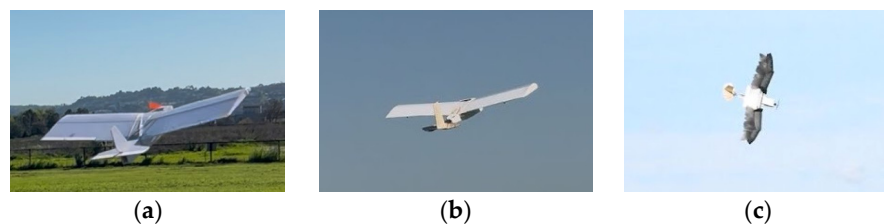


Figure 16. Flight tests: (a) Traditional model, (b) SMART Hawk tail, and (c) SMART Hawk.

5. Summary and Conclusions

This paper presents the design of SMART Hawk, a non-flapping UAV inspired by the flight characteristics of the red-tailed hawk. A series of mathematical models were created in MUX, along with CFD simulations in ANSYS Fluent, to size the drone and examine the effects of the wing feathers on the generated lift and drag. An avian-inspired wing mechanism was designed with two DOFs, enabling asymmetric tucking for roll generation, and three DOFs in the tail consisting of roll, pitch, and feather expansion. Prototypes of all subsystems were manufactured and assembled. Flight testing showed that the morphing tail has sufficient authority to steer the model without ailerons and that SMART Hawk's feathered wing and tail can achieve sustained flight with the selected propulsion and actuation systems. Future work will include more flight tests and analysis of flight

data to characterize the flight performance. In addition, a virtual model of SMART Hawk will be integrated into a flight simulator to aid in pilot training before actual flight tests.

Supplementary Materials: The following supporting information can be downloaded at: <https://www.mdpi.com/article/doi/s1>, Video S1: SMART Hawk design and flight tests.

Author Contributions: Conceptualization, L.H., V.B., C.W. and P.L.B.; methodology, all authors; software, all authors; validation, L.H., V.B., C.W. and P.L.B.; formal analysis, L.H., C.W., A.G., A.S. and P.L.B.; investigation, L.H., V.B., C.R., G.V., N.A., E.H., C.G., C.L., A.A., R.B., J.M. and L.A.; resources, P.L.B.; data curation, L.H., V.B., C.W. and P.L.B.; writing—original draft preparation, all authors; writing—review and editing, L.H., V.B., C.W. and P.L.B.; visualization, all authors; supervision, P.L.B.; project administration, L.H., V.B., C.W. and P.L.B.; funding acquisition, P.L.B. All authors have read and agreed to the published version of the manuscript.

Funding: This research received no external funding.

Data Availability Statement: The raw data supporting the conclusions of this article will be made available by the authors on request.

Acknowledgments: This work was done by the tenth cohort of the “Smart Morphing Wing” research-based senior design project at California State University, Northridge (CSUN). The authors acknowledge the support of the following members: Mark Thomas, Ryan Thomas, Isaac Aguilar, Jesus Gonzales Barrera, Christian Avendano, and Samuel Min. The authors acknowledge the Mechanical Engineering Department, the Instructionally Related Activities (IRA) grant, and the Student Travel and Academic Research (STAR) program at CSUN.

Conflicts of Interest: The authors declare no conflicts of interest.

References

1. Andreson, J. *Introduction to Flight*, 8th ed.; McGraw Hill: Columbus, OH, USA, 2015.
2. Cartron, J.-L.E. *Raptors of New Mexico*; University of New Mexico Press: Albuquerque, NM, USA, 2010.
3. Bamford, C.; Swiney, P.; Nix, J.; Hedrick, T.L.; Raghav, V. Aerodynamic Response of a Red-Tailed Hawk to Discrete Transverse Gusts. *Bioinspir. Biomim.* **2024**, *19*, 036011. <https://doi.org/10.1088/1748-3190/ad3264>.
4. Tanaka, S.; Asignacion, A.; Nakata, T.; Suzuki, S.; Liu, H. Review of Biomimetic Approaches for Drones. *Drones* **2022**, *6*, 320. <https://doi.org/10.3390/drones6110320>.
5. Ajanic, E.; Paolini, A.; Coster, C.; Floreano, D.; Johansson, C. Robotic Avian Wing Explains Aerodynamic Advantages of Wing Folding and Stroke Tilting in Flapping Flight. *Adv. Intell. Syst.* **2023**, *5*, 2200148. <https://doi.org/10.1002/aisy.202200148>.
6. Murayama, Y.; Nakata, T.; Liu, H. Aerodynamic Performance of a Bird-Inspired Morphing Tail. *J. Biomech. Sci. Eng.* **2023**, *18*, 22–00340. <https://doi.org/10.1299/jbse.22-00340>.
7. Zhang, H.; Yang, H.; Dang, Q.; Wang, G.; Song, C.; Yang, C. Unsteady Aerodynamics of Elastic Avian-Inspired Morphing Wing during the Folding Process. *Aerosp. Sci. Technol.* **2026**, *173*, 111776. <https://doi.org/10.1016/j.ast.2026.111776>.
8. Ajanic, E.; Feroskhan, M.; Wüest, V.; Floreano, D. Sharp Turning Maneuvers with Avian-Inspired Wing and Tail Morphing. *Commun. Eng.* **2022**, *1*, 34. <https://doi.org/10.1038/s44172-022-00035-2>.
9. Chang, E.; Chin, D.D.; Lentink, D. Bird-Inspired Reflexive Morphing Enables Rudderless Flight. *Sci. Robot.* **2024**, *9*, eado4535. <https://doi.org/10.1126/scirobotics.ado4535>.
10. Phan, H.-V.; Floreano, D. A Twist of the Tail in Turning Maneuvers of Bird-Inspired Drones. *Sci. Robot.* **2024**, *9*, eado3890. <https://doi.org/10.1126/scirobotics.ado3890>.
11. Brody, M.; Podell, D.; Corte Garcia, F.; Munoz, E.; Massey, S.; Minassian, E.; Gharibi, N.; Lyon, D.; Sanchez, B.; Bishay, P.L. MataGull: A Lightweight Bio-Inspired Non-Flapping Bird-like Morphing Drone. In *Proceedings of the 2023 Regional Student Conferences*; American Institute of Aeronautics and Astronautics: University at Buffalo, Buffalo, NY, USA, 2023.
12. Bishay, P.; Rini, A.; Brambila, M.; Niednagel, P.; Eghdamzmiri, J.; Yousefi, H.; Herrera, J.; Saad, Y.; Bertuch, E.; Black, C.; et al. CGull: A Non-Flapping Bioinspired Composite Morphing Drone. *Biomimetics* **2024**, *9*, 527. <https://doi.org/10.3390/biomimetics9090527>.

13. Swiney, P.A.; Wietstruk, M.; Gosdin, L.; Bellah, J.; Raghav, V. Preliminary Investigation of the Aerodynamic Response of a Red-Tailed Hawk to a Vertical Gust. In *Proceedings of the AIAA Scitech 2020 Forum*; American Institute of Aeronautics and Astronautics: Orlando, FL, USA, 2020.
14. Menter, F.R. Two-Equation Eddy-Viscosity Turbulence Models for Engineering Applications. *AIAA J.* **1994**, *32*, 1598–1605. <https://doi.org/10.2514/3.12149>.
15. King, A.S.; McLelland, J. *Birds: Their Structure and Function*, 2nd ed.; Baillière Tindall: London, UK, 1984.
16. Avian Osteology. Available online: https://rbcm.ca/Natural_History/Bones/Species-Pages/RTHA.htm (accessed on 21 February 2026).
17. Red-Tailed Hawk (Rio Bosque Wetlands Biological Treasure Hunt) iNaturalist. Available online: https://www.inaturalist.org/guide_taxa/377326 (accessed on 21 February 2026).

Disclaimer/Publisher's Note: The statements, opinions and data contained in all publications are solely those of the individual author(s) and contributor(s) and not of MDPI and/or the editor(s). MDPI and/or the editor(s) disclaim responsibility for any injury to people or property resulting from any ideas, methods, instructions or products referred to in the content.